Taylor & Francis
Taylor & Francis Group

Separation Science and Technology

ISSN: 0149-6395 (Print) 1520-5754 (Online) Journal homepage: www.tandfonline.com/journals/lsst20

Comparison of structural properties and removal behavior of composites containing chitosan and hexagonal boron nitride in different compositions

Abdullah Duzgun & Sahra Dandil

To cite this article: Abdullah Duzgun & Sahra Dandil (2023) Comparison of structural properties and removal behavior of composites containing chitosan and hexagonal boron nitride in different compositions, Separation Science and Technology, 58:14, 2556-2577, DOI: 10.1080/01496395.2023.2258277

To link to this article: https://doi.org/10.1080/01496395.2023.2258277

SEPARATION SCIENCE AND TECHNOLOGY
2023, VOL. 58, NO. 14, 2556–2577
https://doi.org/10.1080/01496395.2023.2258277

Taylor & Francis
Taylor & Francis Group

Comparison of structural properties and removal behavior of composites containing chitosan and hexagonal boron nitride in different compositions

Abdullah Duzgun and Sahra Dandil

Department of Chemical Engineering, Faculty of Engineering, Bilecik Şeyh Edebali University, Bilecik, Türkiye

ABSTRACT

This study aims to prepare different possible composites using hBN and chitosan in varying ratios and compare them with each other. Composites c/hBN:100/0, c/hBN:75/25 and c/hBN:50/50 were prepared in varying mass ratios. Depending on the changing mass composition, the characterization results are presented in comparison with each other. The surface structures were observed by SEM analysis. FTIR analysis was used for functional group determination. Surface and pore identification was carried out by BET analysis. Crystalline formations were revealed by XRD analysis. True density values were determined by pycnometric analysis. Also, the RB 49 dye removal behavior of the composites was examined and compared with each other. c/hBN:100/0 and c/hBN:75/25 showed the highest removals at pH 4 and as 86.53 and 90.2%, respectively, while c/hBN:50/50 showed it at pH 3 and as 86.59%. The highest adsorption capacities were determined as 105.28, 160.71 and 159.01 mg/g for c/hBN:100/0, c/hBN:75/25 and c/hBN:50/50, respectively at 0.3 g/L dosage. The pseudo-second-order kinetic model and intraparticle diffusion model fitted well with the processes over time. The Freundlich isotherm model was found to be compatible with the processes. The positive ΔH and ΔS values and negative ΔG values of each process were presented.

ARTICLE HISTORY
Received 12 May 2023
Accepted 7 September 2023

KEYWORDS
Characterization; comparison; composite; RB 49; removal

Introduction

In general terms, composite material is a material in which properties that cannot be obtained with an individual component can be obtained by combining more than one component with different properties.[1] It can gain improved properties compared to its components. Strength, hardness, toughness, corrosion resistance and thermal insulation are examples of these properties.[2] Composite materials attract attention with their features such as selecting components and adapting them to obtain the required properties, and therefore they are in almost every field.[3]

After the technological revolution, in addition to serious air and soil pollution, the pollution of water, which is indispensable for living life, has approached critical levels.[4] Wastewater containing various harmful pollutants causes a danger to human life and the ecosystem.[5] There are different methods to improve water quality by removing or recovering pollutants from wastewater, including membrane technique, biological treatment, precipitation and adsorption.[6,7] Among these techniques, although effective separation is achieved in membrane processes, sludge production is a disadvantage of the method. Biological treatment, on the other hand, can be operated at a low cost, but the process is slow and can be used for limited applications.-[8] For the precipitation method, which is an established method, the use of high amounts of chemicals and its negative effects on health cause problems in its usage.[9] Although the removal of the adsorbent is a disadvantage in adsorption, it is considered advantageous over other techniques due to its low energy requirement, low cost of operation, no pre-treatment, simplicity and efficiency.[8,10,11] In water treatment, adsorption takes place as the pollutant adheres to the surface of the solid adsorbent. Adsorbent and its physicochemical properties highly affect the practicality of the process.[12] In the literature, there are many removal studies in which different adsorbents have been developed for various pollutants. Ali et al. used multi-walled carbon nanotubes for the adsorption of fenuron pesticide, which is a long-lasting agricultural toxic substance, and they argued that the method is fast, low-cost, effective and reproducible.[13] For the decolorization of waters containing methylene blue, malachite green, and crystal violet dyes, Alqadami et al. blended jackfruit peel into sugarcane bagasse powder. They studied the variation of the parameters affecting the adsorption and reached

CONTACT Sahra Dandil sahra.ugur@bilecik.edu.tr Department of Chemical Engineering, Faculty of Engineering, Bilecik Şeyh Edebali University, Bilecik 11100, Türkiye

high adsorption capacities depending on the parameters.[14] Khan and coworkers developed a magnetic copper ferrite/drumstick pod composite using ferrites and drumstick pod biomass, which are known for their fast adsorption kinetics and efficiency and demonstrated their effectiveness in lead and malachite green removal. They demonstrated that the composite could efficiently and cost-effectively remove lead and malachite.[15] Azam et al. treated the waste ajwa date pits with H_2O_2 as a high-efficiency and cost effective material for the adsorption of Cu(II) ions. As a result of the study, they explained that they developed a method with high adsorption and desorption efficiency that can be used for heavy metal ions as well as other pollutants.[16]

Increasing the performance of adsorption processes with the production of more effective adsorbents by preparing composites has attracted attention as an area where composite materials are frequently used in recent years.[17] Composite adsorbents can be prepared by physical or chemical methods. In the physical method, a homogeneous mixture is obtained by mixing or impregnating all components by using ultrasonication and magnetic stirring. In the chemical method, a chemical reaction occurs during the preparation of the adsorbent.-[18] Although many natural or chemical materials are used in the preparation of composites, it is primarily preferred to obtain efficient and low-cost adsorbents with natural materials. Chitosan, a natural polymer, is widely used in the preparation of composite adsorbents with its functional groups suitable for adsorption.[19,20]

Boron nitride is a material that does not occur naturally and is produced synthetically from B and N. It is isoelectronic and isostructural to carbon.[21] hBN is one of the forms of BN and attracts attention with its stability and layered structure. B and N atoms coexist by covalently bonding in each layer, and van der Waals forces are active in the layers.[22] The strong affinity between B and N makes hBN mechanically robust and thermally insulating.[23]

This study aimed to prepare stable composites with possible compositions with chitosan and hBN and determine the properties that different compositions change in composites and compare them with each other. To examine the effect of the composition ratio in the composites, different mass ratios of the components were used. For c/hBN ratios, as mass percent c/hBN:100/0, c/hBN:75/25, c/hBN:50/50, c/hBN:25/75 and c/hBN:0/100 composite solutions were prepared. At c/hBN:25/75 and c/hBN:0/100 ratios, the components remained dispersed in the aqueous medium and no composite formation was observed, while stable composites were obtained for c/hBN:100/0, c/hBN:75/25, c/hBN: 50/50 ratios. For this reason, studies on c/hBN:100/0, c/hBN:75/25, and c/hBN:50/50 composites were included in the study. Detailed characterization of the stable composites was performed. According to our best research, the preparation of composites with hBN and chitosan in different compositions and comparison them with each other has not been presented in previous studies. Examining the removal behaviors and comparing them with each other has been selected as an application area for the composites. In a previous study by us, the adsorbing ability of one of the composites was studied for the adsorption of RB3R and RP4BN dyes to investigate the usability of hBN as an adsorbent.[24] In this study, unlike our previous study, new and stable possible composite forms were prepared by testing different ratios of the components. Also, the structural properties of these composites were determined by SEM, FTIR, BET, XRD and He pycnometer analyses and compared with each other. In addition, the removal behavior of the stable composites was also determined and presented in comparison with each other. Since dyes are harmful, toxic, non-degradable and carcinogenic substances that are frequently found in effluents of paper, plastic and textile industries, their removal is very important because they cause great harm to human health, all living things and nature.[25,26] Therefore, it was aimed to remove RB 49 dye from aqueous solutions with stable composites.

Materials and methods

Materials

RB 49 (purity of 99%) was provided from a dye production factory in Bursa, Türkiye. The chemical structure of the RB 49 is given in Fig. 1.[27] HCl (≥37%) was purchased from Fluka (Charlotte, North Carolina, US) and 1, 2 and 5 M HCl solutions were used for pH adjustment of aqueous RB 49 solutions. hBN (micron size) was purchased from Boron Technologies and Mechatronic Ind. Co, Eskisehir, Türkiye. Chitosan was provided by the department in Bilecik, Türkiye. Acetic acid (≥99.8%) was supplied from Fluka (Charlotte, North Carolina, US). Glutaraldehyde solution (50%) was purchased from Fluka (Charlotte, North Carolina, US). Ethanol (absolute) was purchased from Merck (Darmstadt, Germany). NaOH was supplied by Carlo Erba (Milano, Italy). NaCl (≥99.8%) was provided by Sigma Aldrich (Massachusetts, United States).

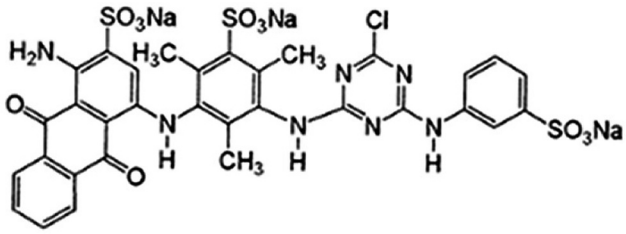

Figure 1. Chemical structure of RB 49 dye.[27]

Methods

Preparation of c/hBN composites at different mass ratios

The method in reference [24] was used as the composite preparation method at different mass ratios. A 5% by-volume acetic acid solution was prepared and chitosan was added to it. The mixture was left to stir overnight in a magnetic stirrer (IKA C-MAG HS 7, Staufen, Germany). Then, hBN was added to the mixture as c/hBN:100/0, c/hBN:75/25 and c/hBN:50/50 by mass percent. A 1 M NaOH solution was also prepared. The mixture containing chitosan and hBN was added dropwise to the NaOH solution, which was allowed to stir at low speed in the magnetic stirrer, and was stirred overnight. After mixing was complete, the resulting particles were washed several times. A 2.5% by mass glutaraldehyde solution was prepared with ethyl alcohol. The washed particles were added to this solution and reacted at 60°C for 15 h. After 15 h, the composites were washed again. Then, they were cooled down at −80°C (Nüve DF 490, Ankara, Türkiye) for 1 night. The composites were taken in a freeze dryer (Labconco FreeZone 2.5, Kansas, Missouri, US) for 24 h.

Determination of the pzc of the c/hBN composites

Experiments for the determination of pzc were conducted similarly to previous studies.[28,29] The pzc of c/hBN:100/0, c/hBN:75/25 and c/hBN:50/50 composites were determined using 0.01 M NaCl solution. 50 mL of NaCl solution was taken in seven flasks. The pH values of the NaCl solutions were adjusted as pH 1, 3, 5, 7, 9, 11 and 13. 0.025 g of one of the composites was put in the flasks and shaken for 24 h at 120 rpm. After 24 h, the pH of the solutions was determined and recorded. The same procedure was repeated for all composites.

Removal experiments

Studies for the removal of RB 49 dye by the c/hBN:100/0, c/hBN:75/25 and c/hBN:50/50 composites were carried out with 50 mL synthetic dye solutions. A shaker (Termal H11960, Istanbul, Türkiye) at a constant shaking speed of 200 rpm was used for experiments. The effective parameters of the processes were studied under the following conditions:

To investigate the effect of the pH of RB 49 dye solution and contact time on the dye removal processes were investigated simultaneously. The behavior of the processes was followed in the range of pH 1–5 of the dye solutions for 240 min. Experiments were performed at 60 ppm RB 49 dye concentration, 0.5 g/L composite dosage and room temperature.

Dosage studies were performed for c/hBN:100/0, c/hBN:75/25 and c/hBN:50/50 composites in the range of 0.3–0.7 g/L at 60 ppm dye solution concentration. The experiments were followed for 240 min at room temperature.

To examine the effect of initial dye concentration on the RB 49 dye removal by the c/hBN composites, dye solutions in the range of 20–100 ppm were prepared. Experiments were carried out at 0.3 g/L composite dosage and room temperature for 240 min for each concentration.

To investigate the temperature effect on the RB 49 dye removal, experiments were performed in the range of 25–45°C. The removal efficiencies were defined at each temperature for 60 ppm initial dye concentration and 0.3 g/L composite dosage and at the equilibrium time.

To determine the RB 49 dye concentrations in aqueous solutions, samples were taken from the solutions at specified time intervals. A UV-Vis spectrophotometer (Perkin Elmer, Elmer Analyst 800, Waltham, Massachusetts, United States) was used at 586 nm to determine the absorbance values of the samples.

Equations

The removal efficiency and q_e values for the RB 49 removal processes were calculated as in Equations (1) and (2), respectively:[30]

$$\text{Removal efficiency}(\%) = \frac{(C_0 - C_e)x100}{C_0} \qquad (1)$$

$$q_e\left(\frac{mg}{g}\right) = \frac{(C_0 - C_e)xV}{m} \quad (2)$$

The kinetic studies of the adsorption processes were investigated using the pseudo-first-order, pseudo-second-order and intraparticle diffusion models. Equations (3), (4) and (5) belong to the mentioned models, respectively:[31]

$$q_t = q_e(1 - \exp(K_1 t)) \quad (3)$$

$$q_t = \frac{K_2 q_e^2 t}{1 + K_2 q_e t} \quad (4)$$

$$q_t = K_i t^{0.5} + C \quad (5)$$

Adsorption equilibrium isotherms were studied with Langmuir and Freundlich isotherms. Langmuir and Freundlich isotherm models are formulated in Equations (6) and (7), respectively.[32]

$$q_e = \frac{q_m K_L C_e}{1 + K_L C_e} \quad (6)$$

$$q_e = K_F C_e^{\frac{1}{n}} \quad (7)$$

The following equations are used for thermodynamic analysis[33]:

$$\ln K_a = \frac{\Delta S^\circ}{R} - \frac{\Delta H^\circ}{RT} \quad (8)$$

$$K_a = \frac{q_e}{C_e} \quad (9)$$

$$\Delta G^\circ = \Delta H^\circ - T\Delta S^\circ \quad (10)$$

Characterization techniques

SEM (Zeiss Supra 40VP, Oberkochen, Baden-Württemberg, Germany) analysis was used to investigate the surface of the c/hBN composites. Chemical characterization of the c/hBN composites was studied with the FTIR technique and analyses were performed with a Perkin Elmer LR64912C (Waltham, Massachusetts, United States) device. BET analysis (Micromeritics Asap 2020, Greater Atlanta Area, East Coast, Southern US) provided information on the surfaces and the pore states under N_2 atmosphere at 77 K. Degas temperature defined as 80°C and time for 6 h. XRD analysis was performed using Panalytical Empyrean (Malvern, United Kingdom) device for 2θ = 5–60 ° to determine the crystallinity of the composites. He pycnometer (Micromeritics Accupyc II 1340, Greater Atlanta Area, East Coast, Southern US) was used to determine the true density of the composites.

Results and discussion

SEM, FTIR, BET, XRD and pycnometer analyses

SEM analysis

The properties and structure of the surface are major factors related to the performance of the removal processes. SEM analyses were performed for chitosan and hBN, which have different mass ratios in the composition of the c/hBN composites, and the SEM images are presented in Figures 2(a,b), respectively. The surface of the composites was also investigated by SEM analysis. SEM images obtained at different magnifications to observe the appearance and surface of a composite particle for c/hBN:100/0, c/hBN:75/25 and c/hBN:50/50 composites are given in Figures 2(c-e), respectively. In addition, SEM images of c/hBN:100/0, c/hBN:75/25 and c/hBN:50/50 composites after RB 49 dye adsorption were taken to observe the surface appearance of the composites after adsorption, are shown in Fig. 2(f-h), respectively.

The surface structures of chitosan and hBN are seen in the SEM images given in Figures 2(a,b), respectively, and it was determined that the surface of hBN was flaky, while the chitosan had a non-porous surface. In the low-magnification SEM images of the general view of the composite particles in Figures 2(c-e), it is seen that the composites are spherical, regular and stable. Again, according to these figures, it has been determined that the composite particles form stable for the ratios of 100/0, 75/25 and 50/50 by the mass percentage of c/hBN and these ratios are adequate for forming composites. However, as shown in the high-magnification SEM images of the composites seen in the same figures, it is seen that the surfaces are porous and homogeneous. Accordingly, it was determined that a porous and uniform surface was obtained for the preparation of composites, different from the surface structures of the components of the composites. It has also been shown in the study by Spoială that the prepared composites show different surface structures from their components.[34] In the SEM images in Figures 2(f-h), homogeneous surfaces were observed for the composites after adsorption. Here, it is seen that most of the pores, which appear empty in the images before the adsorption of each composite, are closed after adsorption. This explains that the pores are filled with RB 49 dye molecules, as in previous studies in the literature.[35,36]

FTIR analysis

FTIR analyses were performed for the functional group determination of c/hBN:100/0, c/hBN:75/25 and c/hBN:50/50 composites. The FTIR spectrum of the c/hBN composites is given in Fig. 3(a). In addition, chemical characterization and FTIR analysis of the composites after adsorption were also performed and the spectrum is presented in Fig. 3(b).

It is seen that there are similar peaks at similar wavelengths in the FTIR spectra before and after adsorption for composites in Fig. 3. It has also been encountered in the literature.[37] In addition, the FTIR peaks of chitosan in Fig. 3(a) were obtained similar to a previous study.[38] It was determined that there were some changes in the FTIR spectrum given in Fig. 3(b) compared to the before adsorption. Shifts in the peaks, disappearing and newly formed peaks indicate that adsorption has taken place and new interactions have occurred.[39]

The peaks obtained as 3355.49, 3365.68 and 3356.67 cm^{-1} for c/hBN:100/0, c/hBN:75/25 and c/hBN:50/50 composites, respectively, in the FTIR spectrum for before adsorption given in Fig. 3(a), indicates the stretching vibrations of O – H groups.[40] The 2926–2931 cm^{-1}

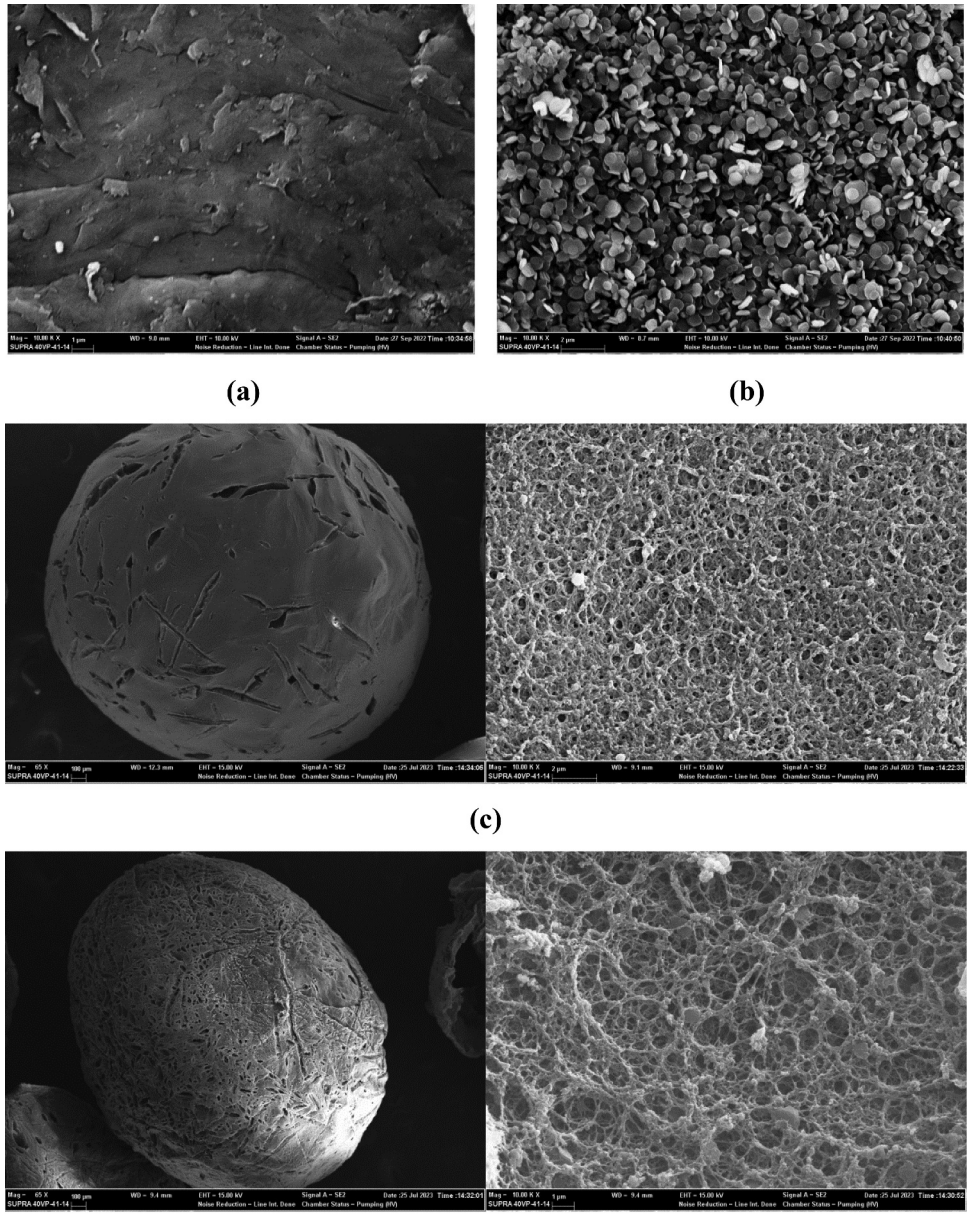

Figure 2. SEM images of (a) chitosan (10.00 KX), (b) hBN (10.00 KX), (c) c/hBN:100/0 composite (65 X and 10.00 KX), (d) c/hBN:75/25 composite (65 X and 10.00 KX), (e) c/hBN:50/50 composite (65 X and 10.00 KX), (f) c/hBN:100/0 composite-AA (20.00 KX), (g) c/hBN:75/25 composite-AA (20.00 KX) and (h) c/hBN:50/50 composite-AA (20.00 KX).

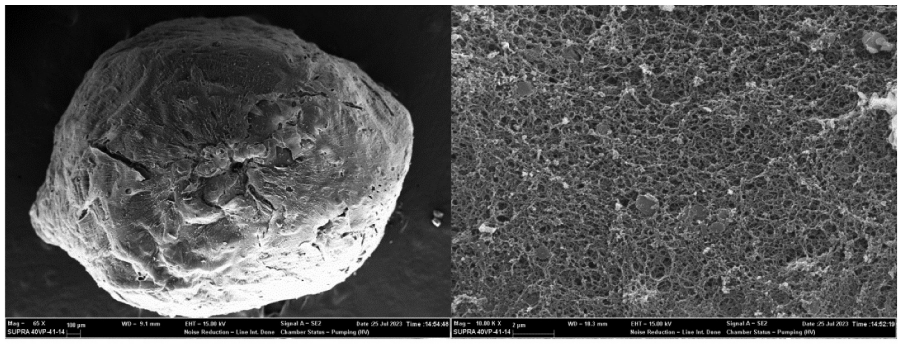

(e)

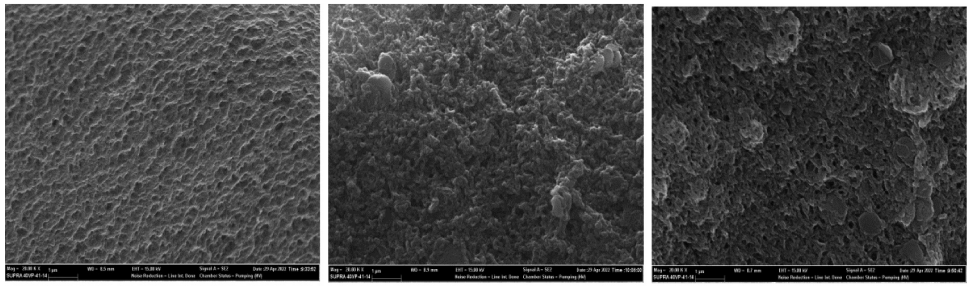

(f) (g) (h)

Figure 2. (Continued).

and 2863–2881 cm^{-1} peaks obtained before adsorption, belong to the asymmetric and symmetric CH_2 stretch vibrations of chitosan, respectively.[41] Due to the interaction with the dye molecules in the aqueous medium, the peaks observed around 3300 cm^{-1} and 2900 cm^{-1} before adsorption were observed as broadened peaks around 3200 cm^{-1} and 2800 cm^{-1} after adsorption. The weak peaks seen at 2161.63, 2180.99 and 2166.96 cm^{-1} for c/hBN:100/0, c/hBN:75/25 and c/hBN:50/50 in Fig. 3(a), respectively, show the C-N interactions in the structure of the composites.[42,43] The C=O stretching bands of chitosan were observed around 1662 cm^{-1} for all composites (Fig. 3(a)).[44] The weakening of the peaks around 1600 cm^{-1} after the adsorption was interpreted as the breaking of the C=O bonds in the structure of the composites. 1559–1561 cm^{-1} peaks for before adsorption show deformation vibrations of $-NH_2$.[45] Again, the weakening of the strong peaks seen around 1500 cm^{-1} after adsorption shows that these bonds have changed. For the c/hBN:100/0 composite without hBN, a small peak is seen at 1401.64 cm^{-1} indicating C-H bending in Fig. 3(a).[46] BN gives a characteristic peak around 1380 cm^{-1}.[47] The peaks obtained in 1383.98 and 1388.10 cm^{-1} of composites containing hBN are enlarged peaks with the contribution of the hBN peak to the C-H bending peak (Fig. 3(a)). After adsorption, peaks were formed in the composites around 1270 cm^{-1}. These peaks may belong to the $-SO_3$ groups in the structure of RB 49.[48] For the after adsorption, only the peak appearing at 1151 cm^{-1} for the c/hBN:100/0 composite belongs to asymmetric $SO4^{2-}$ stretching.[49] The reason why this peak is not observed in other composites may be the strongest binding of dye molecules with c/hBN:100/0. For the c/hBN:100/0, c/hBN:75/25 and c/hBN:50/50 composites after adsorption, 1223.46, 1231.77 and 1219.99 cm^{-1} peaks were formed. These peaks may belong to C-O vibrations.[50–52] The peaks seen at 1027–1029 and 896–900 cm^{-1} in Fig. 3(a), belong to C-O stretching and C-H bending, respectively.[38] These peaks were also seen after adsorption with slight shifts. Due to the characteristic BN peak, strong peaks of around 820 cm^{-1} were observed for c/hBN:75/25 and c/hBN:50/50 before adsorption.[47] In Fig. 3(b), these peaks shifted after adsorption for c/hBN:75/25 and c/hBN:50/50. Many peaks below 800 cm^{-1} were observed after adsorption. These peaks are sulfate peaks showing the adsorption of dye molecules.[53]

BET analysis

The surface area and pore parameters of the composites were investigated by BET analysis. BET surface area,

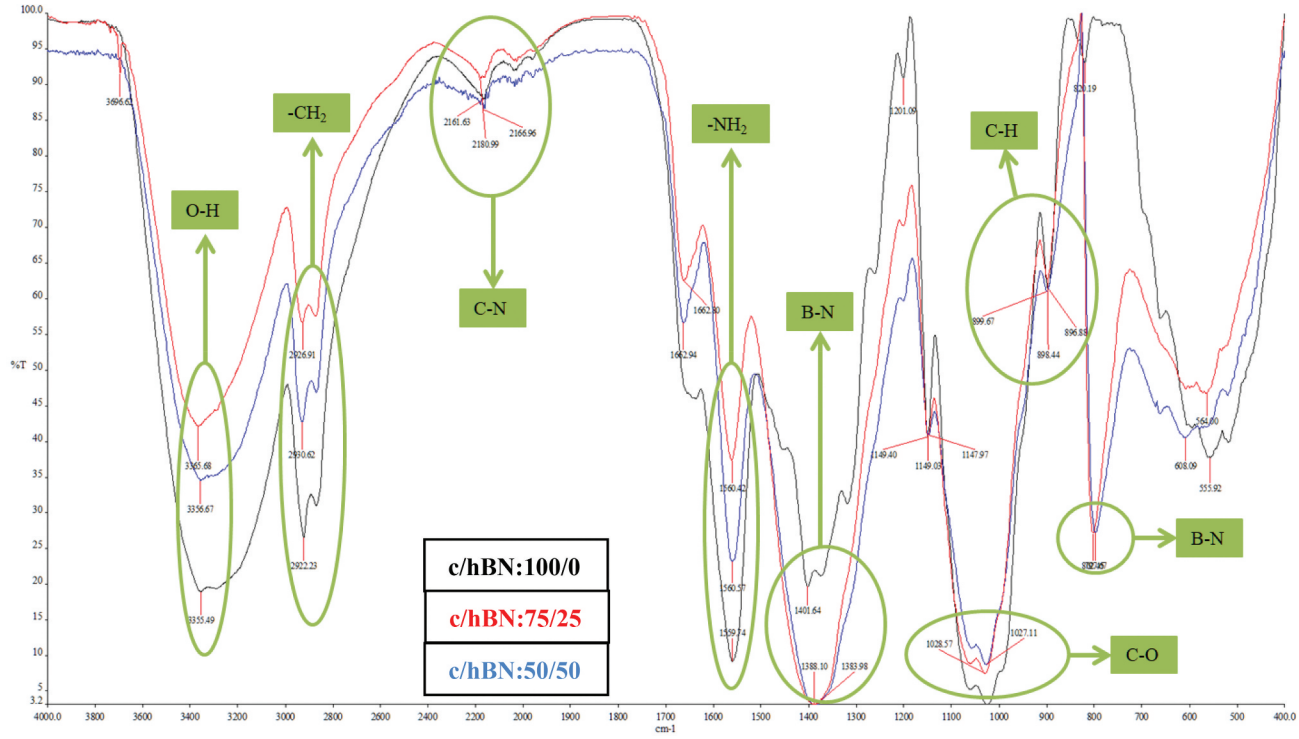

(a)

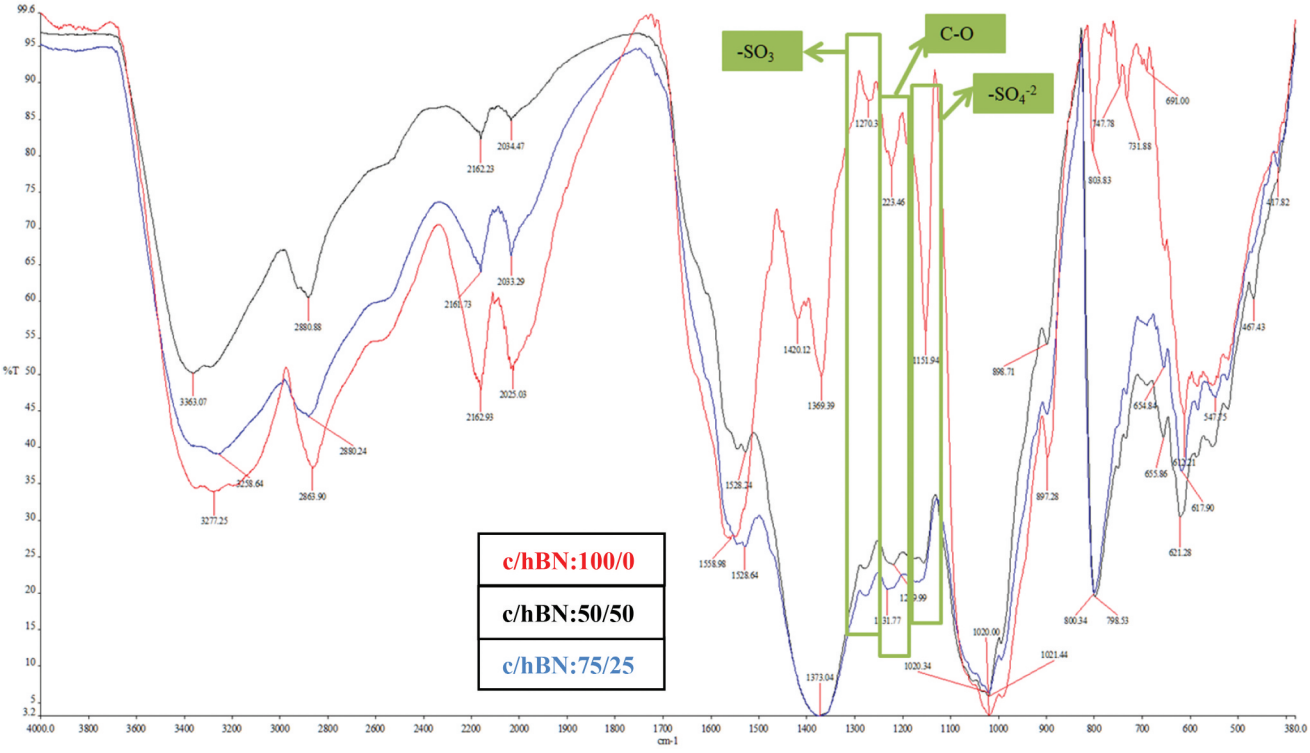

(b)

Figure 3. FTIR spectrum of c/hBN:100/0, c/hBN:75/25 ve c/hBN:50/50 composites for (a) before and (b) after adsorption.

pore volume and pore size values of the composites were given in Table 1. BET surface area for c/hBN:100/0, c/hBN:75/25 and c/hBN:50/50 composites was obtained as 426.30, 80.32 and 65.37 m^2/g, respectively. The pore volumes of c/hBN:100/0, c/hBN:75/25 and c/hBN:50/50 composites were determined as 0.15, 0.035 and 0.029 cm^3/g. Accordingly, the highest surface area and pore volume were obtained for c/hBN:100/0. It was observed that the surface area and pore volume values decreased strongly with the addition of hBN to the chitosan composite, and these values continued to decrease with the increase of the hBN content in the composites. The pore size values were obtained as similar to each other as 21.58, 21.83 and 21.31 Å for the c/hBN:100/0, c/hBN:75/25 and c/hBN:50/50 composites, respectively.

XRD analysis

The crystallinity of the composites was identified by XRD analysis. XRD patterns of the c/hBN:100/0, c/hBN:75/25 and c/hBN:50/50 composites were shown in Figures 4(a), (b) and (c) , respectively. The peaks seen at 10.36 and 20.14° of 2ϴ in Fig. 4(a) show chitosan in crystalline form.[54] As seen in Fig. 4(b), a new and strong peak was observed at 2ϴ 26.87° with the addition of hBN to the composite structure. For c/hBN:75/25 composite, approximately 2ϴ = 10° peak strengthened while 2ϴ = 20° peak weakened. 2ϴ 26.87° peak (002) reflection of hBN. In addition, since the reflection of hBN (001) contributes to the 2ϴ = 10° peak, this peak is strengthened compared to c/hBN:100/0.[55] For the c/hBN:50/50 composite obtained by increasing the amount of hBN in the composite composition, it is seen that the peak at 2ϴ 29.34° is evident and the other peaks are weakened. It can be interpreted that the increased amount of hBN suppresses the peaks of chitosan.

Pycnometry analysis

The volume and true density of the composites were defined by pycnometric analysis. While average volume values for c/hBN:100/0, c/hBN:75/25 and c/hBN:50/50 composites were 0.19, 0.11 and 0.03 cm^3, average density values were determined as 1.70, 2.20 and 3.77 g/cm^3, respectively. Accordingly, with the addition of hBN to the composites, the density increased while the volume decreased.

Table 1. BET analysis results of the composites.

Composite	BET surface area (m^2/g)	Pore volume (cm^3/g)*	Pore size (Å)**
c/hBN: 100/0	426.30	0.15	21.58
c/hBN: 75/25	80.32	0.035	21.83
c/hBN: 50/50	65.37	0.029	21.31

*BJH Adsorption cumulative volume of pores.
**BJH Adsorption average pore width.

Removal studies

Solution pH and time

The pzc defines the solution pH where the positive charges are equal to negative charges on the surface. It is generally considered a characteristic parameter for a surface in an aqueous solution.[56] As given in Fig. 5, the pzc values of c/hBN:100/0, c/hBN:75/25 and c/hBN:50/50 composites were determined as 7.6, 7.4 and 8.4, respectively.

Concentration changes of RB 49 dye in an aqueous solution at each pH value were followed at regular time intervals to determine the dye removal percentages by the c/hBN composites, depending on the solution pH. Figure 6 shows the removal behavior of the c/hBN composites at different pH values depending on time.

As seen in Fig. 6, the equilibrium time was determined as 240 minutes for all processes since the removal efficiencies did not change after 240 minutes in general. Although the removal percentages over time were regular for some pH values and irregular for others, an increasing trend was observed in the removal percentages for all composites. While the removal percentages of the composites were low for pH 1 and 2, they increased for pH 3, 4 and 5. Arab et al. indicated that the capacity increased with increasing pH in the anionic methyl orange dye removal process with zinc curcumin oxide nanoparticles. According to Arab et al., Na^+ in the structure of methyl orange decreased its adsorption capacity by competing with the H^+ ions, which are concentrated in a strongly acidic environment, and positively charged surface of zinc curcumin oxide nanoparticles. Similar to the previous study, RB 49 also contains Na^+. This may be the reason for the low RB 49 removal at pH 1 and 2.[57] According to Figures 6(a) and (b), the highest dye removals for c/hBN:100/0 and c/hBN:75/25 composites were obtained at pH 4 as 86.53% and 90.2%, respectively. For the c/hBN:50/50 composite in Fig. 6(c), the highest removal was achieved at pH 3 as 86.59%. Depending on these results, the composites achieved similar maximum removal percentages at different pH values. The highest removal percentage for c/hBN:50/50 composite with increasing hBN mass ratio was obtained at a different pH value than other composites was evaluated as the increased hBN content of the composite might have affected the surface charge of the composite. In addition,

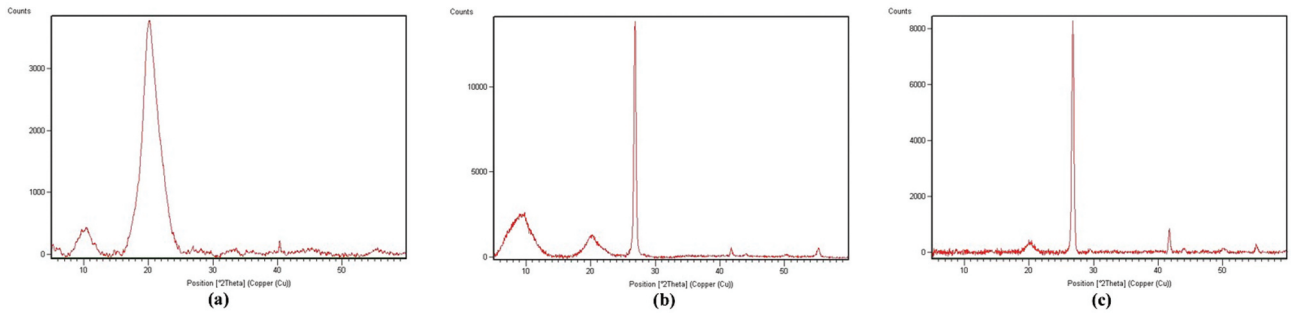

Figure 4. XRD patterns of the (a) c/hBN:100/0, (b) c/hBN:75/25 and (c) c/hBN:50/50 composites.

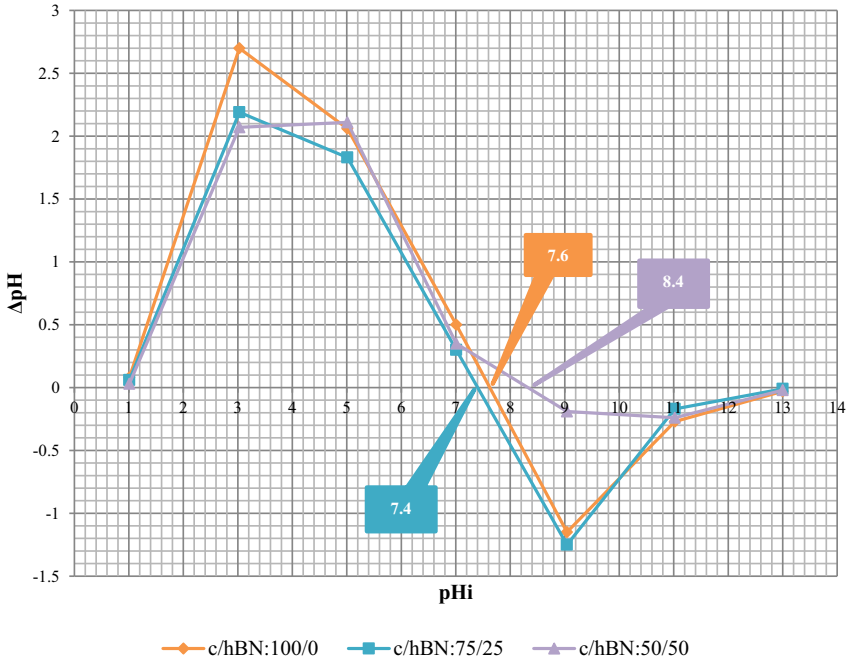

Figure 5. The pzc values of c/hBN composites.

it should be emphasized that the highest removal was achieved with the c/hBN:75/25 composite. Further studies were carried out at pH values where the highest removals were observed for each composite.

As stated above, the pzc values of c/hBN:100/0, c/hBN:75/25 and c/hBN:50/50 composites were determined as 7.6, 7.4 and 8.4, respectively. Accordingly, it was observed that the composites exhibited different surface charges in the aqueous medium by varying amounts of components in their composition. The pzc values of the c/hBN:100/0 and c/hBN:75/25 composites were found to be close to each other and these values were different from the pzc value of the c/hBN:50/50 composite. This may be related to the fact that the pH values at which the highest removals are obtained as the same for the c/hBN:100/0 and c/hBN:75/25 composites and different for the c/hBN:50/50 composite.

If the solution pH is above the pzc, the surface becomes negatively charged and electrostatic attraction causes the adsorption of cations. Conversely, below the pzc values, the density of positive ions on the surface allows anionic species and inhibits cationic species for adsorption.[58] This explains that removal processes of the negative RB 49 dye with composites occur at pHs below the pzc values of each

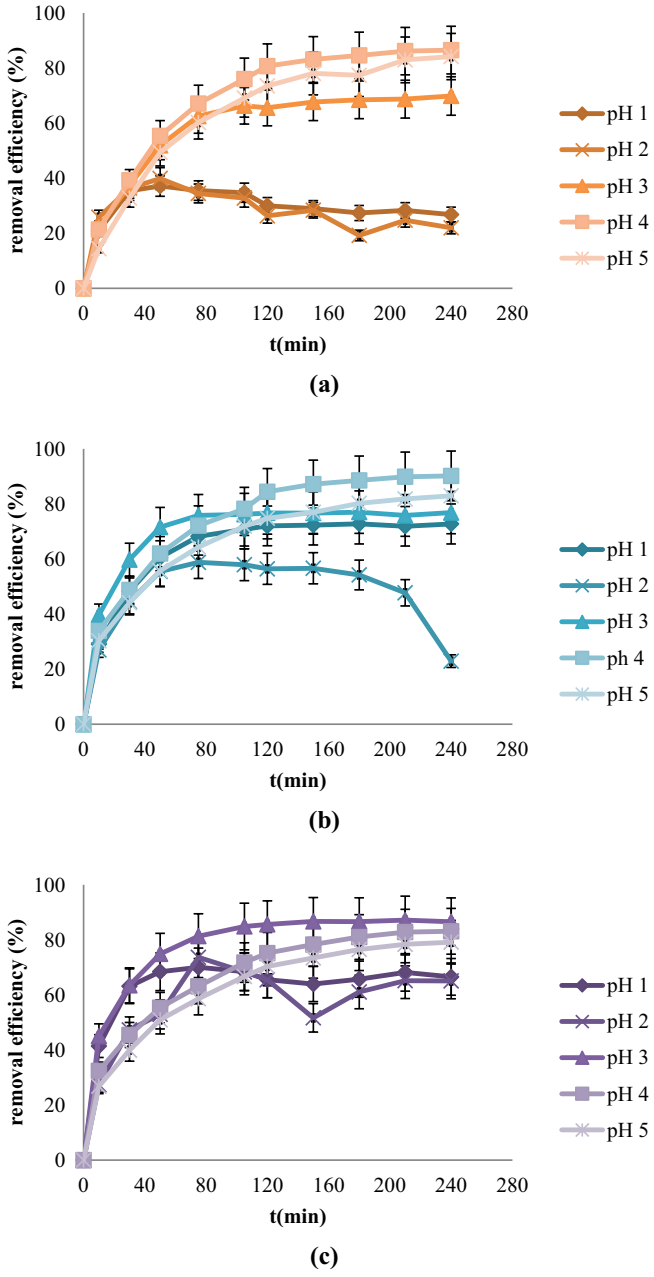

Figure 6. Time- removal efficiency graph of the (a) c/hBN:100/0, (b) c/hBN:75/25 and (c) c/hBN:50/50 composites depending on pH (C_0=60 ppm, composite dosage=0.5 g/L, T=25°C).

composite. In addition, the pzc values, which were 7.6 for the c/hBN:100/0 and 7.4 for c/hBN:75/25, increased to 8.4 when the hBN mass ratio was 50/50. It has been determined that the surface of the c/hBN:50/50 composite in the aqueous medium exhibits a positive character at higher pH values than the other composites.

Composite dosage

The amount of the solid material is one of the effective parameters in removal processes as it increases the active sites. The adsorption capacities of the c/hBN composites at varying dosages of 0.3, 0.5 and 0.7 g/L were followed. The change in the capacities over time for different dosages of the c/hBN composites is shown in Fig. 7.

As seen in Fig. 7, adsorption capacities decreased with increasing composite dosages from 0.3 g/L to 0.7 g/L for all composites. According to Figures 7(a), (b) and (c), the highest adsorption capacities are determined as 105.28, 160.71 and 159.01 mg/g for c/hBN:100/0, c/hBN:75/25 and c/hBN:50/50, respectively at 0.3 g/L composite dosage.

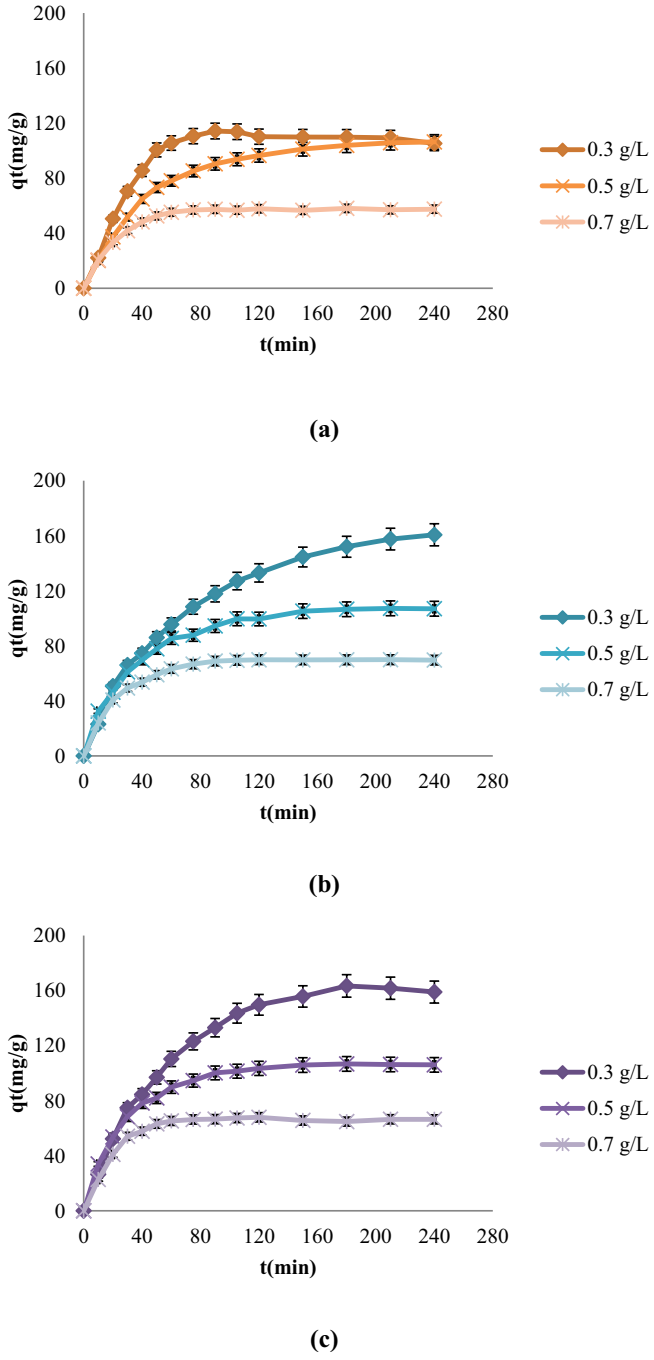

Figure 7. Time- adsorption capacity graph for the (a) c/hBN:100/0, (b) c/hBN:75/25 and (c) c/hBN:50/50 composites (C_0=60 ppm, *t*=240 min, *T*=25°C).

Accordingly, it was determined that the composites showed higher adsorption capacities with hBN added to the composites. An increase in composite amount increases the sites available for the uptake of dye molecules. However, since there will be many active sites, a particularly active site may not reach its maximum adsorption capacity.[59] With the thought that less composite is required by using the active site effectively at low dosages, further studies were carried out with 0.3 g/L dosage of c/hBN composites. Table 2 has been prepared to present the capacity values obtained in this study and other studies in the literature for the removal of RB 49 dye.

Concentration of the dye solution

In adsorption processes, dye concentration changes the efficiency of removal. RB 49 dye solutions were prepared at varying initial concentrations of 20, 40, 60, 80 and 100 ppm and the removal percentages were followed for the

Table 2. Adsorption capacity values of various adsorbents in RB 49 dye removal.

Adsorbent	qe (mg/g)	Reference
c/hBN:100/0	105.28	Present study
c/hBN:75/25	160.71	
c/hBN:50/50	159.01	
chitosan/waste mussel shell composite	54.7	[60]
chitosan/waste mussel shell/waste active sludge char composite	38.8	
chitosan-activated sludge composite particles	16.91	[61]
phytic acid-doped poly-N-phenylglycine@potato peel	216	[62]
a mixed biosorbent of macro-fungus Agaricus bisporus and Thuja orientalis cones	153.26	[63]
thermal decomposition product of alunite-potassium chloride mixture	119.10	[64]
citrus waste	68.61	[65]
biomass obtained from Capsicum annuum seeds	96.35	[66]

equilibrium time (240 min) of the processes. Figure 8 shows the removal behavior of the c/hBN composites at different dye concentrations.

As seen in Fig. 8, composites with different mass ratios in compositions exhibited low removal efficiencies at low concentrations in general, although there were some differences at varying initial dye concentrations. Since the amount of RB 49 dye molecules in the aqueous solution was low at low concentrations, the removal rate was not high, while the removal rate increased as the increasing concentration encouraged mass transfer. However, the increased rate of removal also affected the time to reach equilibrium.[67]

Kinetic studies

The behavior of the processes over time is explained by adsorption kinetic studies.[68] Some mathematical models describe this behavior.[69] The widely studied models are pseudo-first-order, pseudo-second-order and intraparticle diffusion kinetic models. These models were examined to exhibit the removal rate of the RB 49 dye adsorption processes by the c/hBN composites. Figures 9(a-c) are graphs of pseudo-first-order, pseudo-second-order and intraparticle diffusion kinetic models of the processes, respectively. In addition, kinetic parameters are presented in Table 3.

According to Table 3, the R^2 values of the pseudo-second-order kinetic model for adsorption processes with c/hBN:100/0, c/hBN:75/25, and c/hBN:50/50 composites were found as 0.9964, 0.9766, and 0.9892, respectively. These R^2 values were determined to be higher than the R^2 values of the pseudo-first-order kinetic model for all processes. Therefore, the RB 49 dye removal processes were clarified by the pseudo-second-order kinetic model. Additionally, high R^2 values were also observed for the intraparticle diffusion model. Thus, the intraparticle diffusion model is also effective in the processes. As shown in Fig. 9(c), the intraparticle diffusion effect occurs in two stages. According to the R^2 values in Table 3, it was determined that the first step in which the outer surface adsorption takes place is more effective than the second step in which the intraparticle diffusion is controlled for all processes.[70]

Equilibrium isotherms

Adsorption isotherm is a valuable method to understand the adherence of materials on a solid.[71] Equilibrium isotherms of adsorption processes for c/hBN:100/0, c/hBN:75/25 and c/hBN:50/50 composites were investigated by Langmuir and Freundlich isotherm models and related graphs were shown in Figures 10 (a) and (b), respectively. Also, the parameters and correlation coefficients of the equilibrium isotherm models are given in Table 4.

When the isotherm data of Langmuir and Freundlich models are compared in Table 4, higher R^2 values are seen for the Freundlich isotherm model. Thus, it was determined that the equilibrium isotherms of the c/hBN composites were more compatible with the Freundlich isotherm. According to the Freundlich isotherm, dye molecules are adsorbed on the surfaces of c/hBN composites in multilayers.[72] Also, if 1/n values are greater than 1 (*n* value less than 1), common adsorption occurs between active sites with different adsorption capacities, where adsorption takes place spontaneously.[73]

Temperature and thermodynamic studies

The spontaneity and applicability of adsorption processes are determined by thermodynamic studies. Since adsorption is a temperature-dependent process, adsorption processes exhibit different behavior at different temperatures.[74] Studies were performed at 25, 35 and 45°C to investigate the change in the removal percentages of the composites against the changing temperature. Fig. 11 shows the temperature-dependent

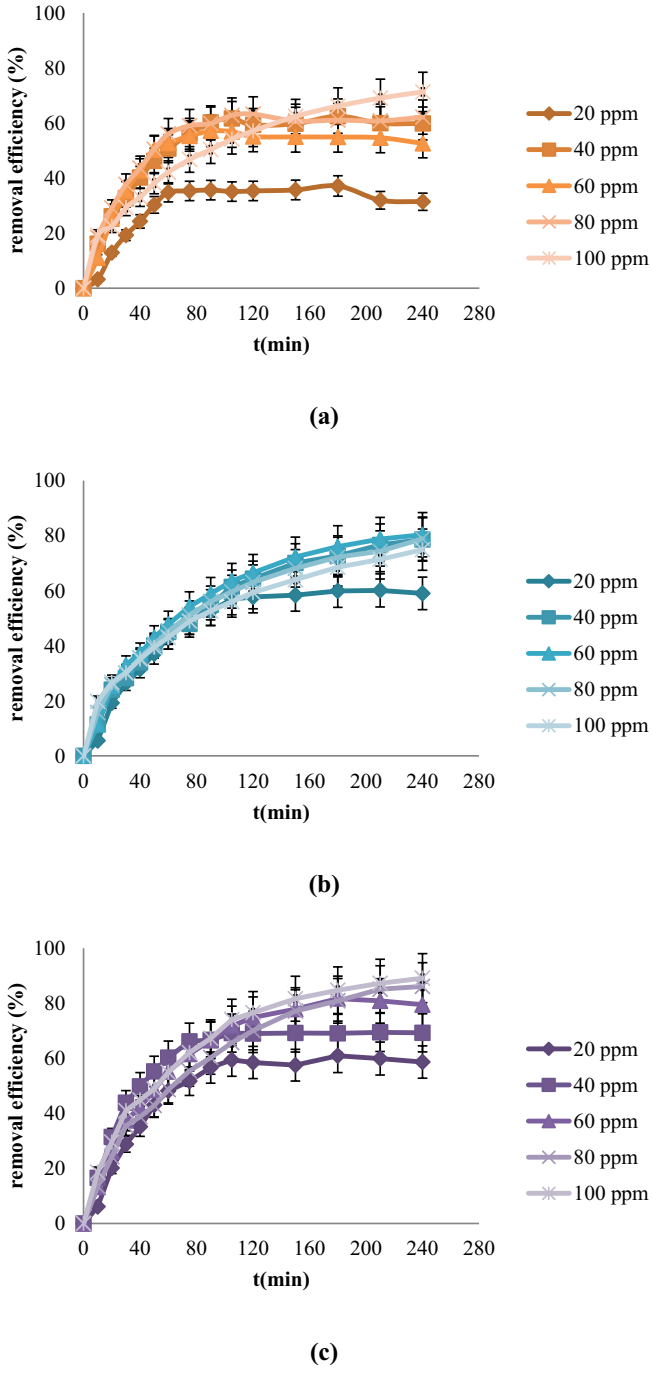

Figure 8. Time - removal efficiency graph depending on initial RB 49 dye concentration for (a) c/hBN:100/0, (b) c/hBN:75/25 ve (c) c/hBN:50/50 composites (composite dosage=0.3 g/L, *t*=240 min, *T*=25°C).

RB 49 dye removal efficiencies of the c/hBN composites. At all temperature values, c/hBN:75/25 and c/hBN:50/50 composites showed high and close removal efficiency, and their efficiency increased slightly with increasing temperature. For the c/hBN:100/0 composite, while the removal efficiency was lower at low temperature compared to other composites, significant increases were observed in the removal efficiency with increasing temperature. As a result, the removal efficiency of all composites increased with increasing temperature. In addition, according to these results, it is clear that the efficiency of composites at low temperatures increased with the addition of hBN to the composite structure. Figures 12 (a), (b) and (c) show the equilibrium constant values against the temperature of the processes of c/hBN:100/0, c/hBN:75/25 and c/hBN:50/50

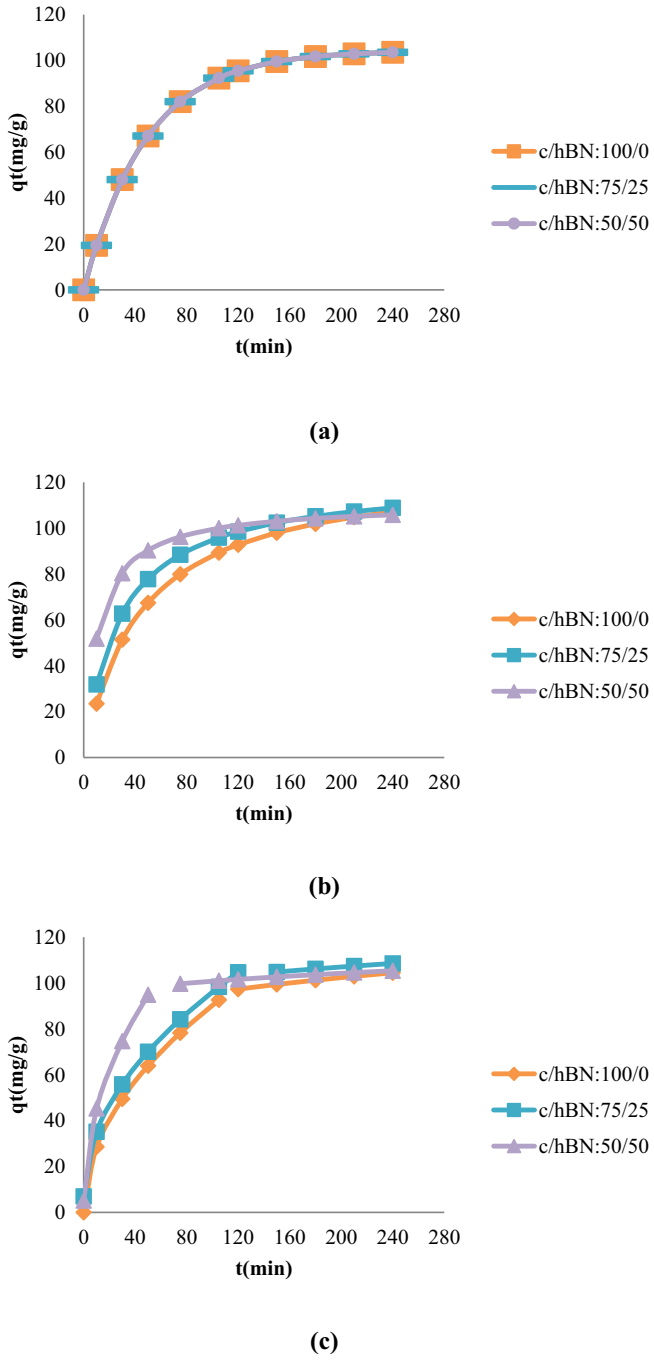

Figure 9. (a) pseudo-first order, (b) pseudo-second-order and (c) intraparticle diffusion model graphs.

composites, respectively. Thermodynamic parameters of the processes were calculated according to the graphs in Fig. 12. ΔH, ΔS and ΔG values for the processes were presented in Table 5.

As represented in Table 5, ΔH values for c/hBN:100/0, c/hBN:75/25 and c/hBN:50/50 composites were found as 53.38, 4.11 and 11.47 kJ/mol, respectively. Positive ΔH values proved the endothermic processes.[75] ΔS values were also found positive for c/hBN:100/0, c/hBN:75/25 and c/hBN:50/50 composites as 190.42, 35.56 and 59.74 J/mol K, respectively. The ΔS values correspond to the more irregular and randomness of the dye molecules on the solid surface compared to the aqueous medium.[76] A high positive ΔS value is known to favor self-adsorption.[77] The highest ΔH and ΔS values were obtained for the process carried out with c/hBN:100/0 composite, and the lowest ΔH and ΔS values were obtained for the process using c/hBN:75/25 composite. In addition, the calculated negative ΔG values for the processes at all temperatures are listed in Table 5. Negative ΔG values represented spontaneous adsorption.[78] For the c/hBN:100/0 composite, the ΔG

Table 3. Parameters of kinetic models.

Kinetic model	Parameter	c/hBN:100/0	c/hBN:75/25	c/hBN:50/50
Pseudo-first order kinetic model	K_1 (x10) (min^{-1})	0.21	0.27	0.56
	$q_{e,\ cal}$ (mg g^{-1})	104.31	105.49	102.01
	R^2	0.9915	0.9364	0.7227
Pseudo-second-order kinetic model	K_2 ($x10^3$) (g mg^{-1} min^{-1})	0.18	0.29	0.79
	$q_{e,cal}$ (mg g^{-1})	126.73	121.64	110.86
	R^2	0.9964	0.9766	0.9892
Intraparticle diffusion model	R^2_1	0.9953	0.9812	0.9722
	R^2_2	0.9650	0.9567	0.7027
	$K_{i,1}$ (mg $g^{-1}min^{-0,5}$)	9.04	8.92	12.69
	$K_{i,2}$ (mg $g^{-1}min^{-0,5}$)	1.57	1.15	0.83
	C_1 (mg g^{-1})	0	6.99	5.15
	C_2 (mg g^{-1})	80.18	90.75	92.50

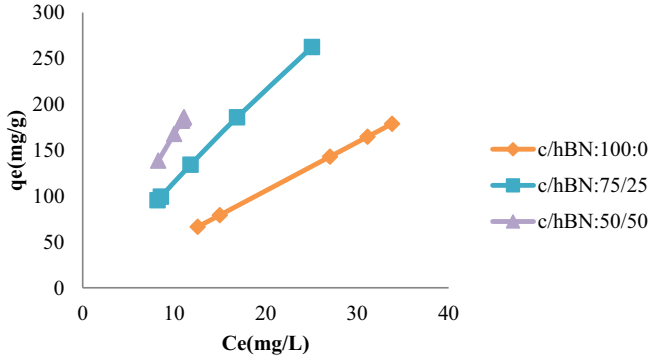

(a)

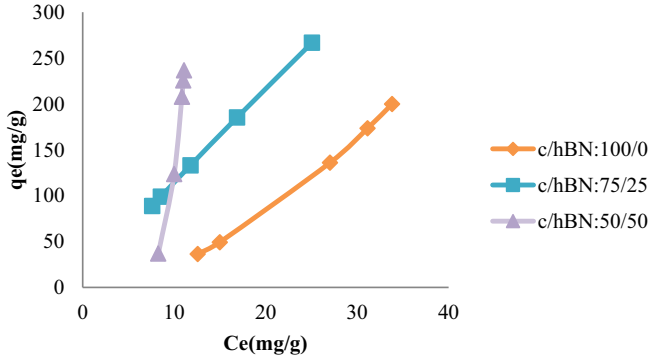

(b)

Figure 10. (a) Langmuir and (b) Freundlich equilibrium isotherms.

Table 4. Equilibrium isotherm data.

Composite	Langmuir Isotherm			Freundlich Isotherm		
	K_L (x10^6) (L mg^{-1})	q_m (x10^{-4}) (mg g^{-1})	R^2	K_F (mg g^{-1} $(L/g)^{1/n}$)	n	R^2
c/hBN:100/0	2.58	205.17	0.7954	0.47	0.58	0.8879
c/hBN:75/25	7092	0.17	0.8340	13.69	1.08	0.8512
c/hBN:50/50	2.31	727.15	0.2790	$5.88x10^{-5}$	0.16	0.7008

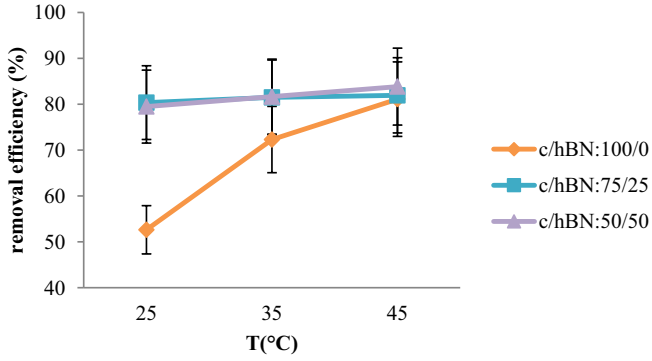

Figure 11. RB 49 dye removal efficiencies of c/hBN composites with temperature.

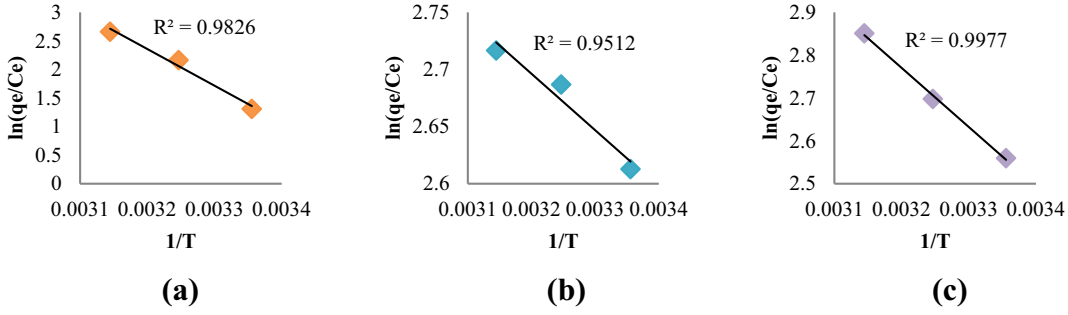

Figure 12. $\ln(q_e/C_e)$-1/T graphs of (a) c/hBN:100/0, (b) c/hBN:75/25 ve (c) c/hBN:50/50 composites.

Table 5. Thermodynamic data.

Composite	T (K)	ΔG (kJ mol^{-1})	ΔH (kJ mol^{-1})	ΔS (J $mol^{-1}K^{-1}$)
c/hBN:100/0	298	−3.37	53.38	190.42
	308	−5.27		
	318	−7.18		
c/hBN:75/25	298	−6.49	4.11	35.56
	308	−6.85		
	318	−7.20		
c/hBN:50/50	298	−6.33	11.47	59.74
	308	−6.93		
	318	−7.53		

values became more negative with increasing temperature. For c/hBN:75/25 and c/hBN:50/50 composites, although ΔG values close to each other were obtained at all temperatures, negativity increased slightly with increasing temperature. ΔG values with increasing negativity indicate that the temperature encouraged spontaneous adsorption.[78,79] Accordingly, the removal efficiency increased with increasing temperature for all composites.[79] At low temperatures, c/hBN:75/25 and c/hBN:50/50 composites have higher negative ΔG values and therefore higher removal efficiencies than composite c/hBN:100/0. These results are consistent with the behavior of the composites given in Fig. 11.

Conclusion

In this study, it is aimed to prepare c/hBN composites with possible different compositions and compare them with each other. Stable composites were obtained at c/hBN:100/0, c/hBN:75/25 and c/hBN:50/50% mass ratios by using varying amounts of chitosan and hBN. The characterizations of the composites were determined in detail by various techniques and compared with each other. Also, investigating the removal behaviors and comparing them with each other has been selected as an application area for the composites. To examine the removal behavior of the composites, RB 49 dye removal studies were carried out. The conclusions of the study are as follows:

- The porous and uniform surface structure of c/hBN composites, as well as the surface of hBN and chitosan, were observed by SEM images. In addition, it was determined in SEM analyses that the dye molecules covered the surfaces after adsorption.
- Functional groups that are similar to each other on the surfaces of the composites for both before adsorption and after adsorption were revealed by FTIR analysis. Slight shifts were detected in some peaks depending on the composition of the composites. In addition, peak disappearances and new peak formations were observed after adsorption, indicating that removal had taken place.
- The surface area and pore parameters of the composites were investigated using BET analysis. In BET analysis, it was observed that the c/hBN:100/0 composite exhibited the highest surface area and pore volume values and these values decreased with increasing hBN content in the composites.
- XRD analyses showed the crystalline formations of the composites. Different peak appearances were observed depending on the composition.
- Pycnometer analyses indicated that increasing hBN in composites increased the true density. Thus, c/hBN:50/50 composite demonstrated the highest true density value than other composites.
- pH-time studies exhibited that the highest removals were determined at pH 4 for the c/hBN:100/0 and c/hBN:75/25 composites as 86.53% and 90.2%, respectively and pH 3 for the c/hBN:50/50 composite as 86.59%. The processes reached equilibrium at 240 min.
- In dosage studies, it was presented that the capacity of the composites containing hBN is higher and the highest adsorption capacities were obtained for the composites at 0.3 g/L dosage as 105.28, 160.71 and 159.01 mg/g for c/hBN:100/0, c/hBN:75/25 and c/hBN:50/50, respectively.
- Higher removal percentages were obtained at higher concentrations due to increased mass transfer with increasing initial dye concentration for all processes.
- In the kinetic studies of each process, it was observed that the processes were compatible with the intraparticle diffusion model as well as the pseudo-second-order kinetic model.
- Compliance of the processes with the Freundlich isotherm model revealed that multilayer adsorption took place.
- In temperature-depend studies, according to positive ΔH and ΔS values and negative ΔG values of the processes, it was determined that the processes were endothermic, the randomness increased at the interface and the adsorption took place spontaneously.

The results showed that it is possible to prepare more than one stable c/hBN composites with different compositions of chitosan and hBN and these composites could be used with high efficiency in RB 49 dye removal. In future studies, c/hBN composites can be tested to remove different pollutants and the effectiveness of each composite can be presented. In addition, composites can be prepared with a different component instead of chitosan and their properties can be studied.

Disclosure statement

No potential conflict of interest was reported by the author(s).

Funding

This work was supported by Bilecik Şeyh Edebali University Scientific Research Projects Coordinatorship [project code: 2021-02.BŞEÜ.03-03].

Abbreviations/Nomenclatures

Abbreviation/Nomenclature	Full name
q_e	adsorption capacity
AA	after adsorption
B	boron
BN	boron nitride
BET	Brunauer–Emmett–Teller
c/hBN	chitosan/ hexagonal boron nitride
C	constant
Cu(II)	copper ion
R^2	correlation coefficient
K_a	distribution coefficient
q_t (mg/g)	dye amount adsorbed at anytime
C_e (mg/L)	dye concentration at equilibrium
C_0 (mg/L)	dye concentration at initial
ΔH (kJ/mol)	enthalpy change
ΔS (kJ/mol K)	entropy change
FTIR	Fourier transform infrared spectroscopy
K_F ($mg^{1-n}.g^{-1}L^{-n}$)	Freundlich model constant
R (8.314 J/mol K)	gas constant
ΔG (kJ/mol)	Gibbs free energy change
He	helium
n^{-1}	heterogeneity factor
hBN	hexagonal boron nitride
HCl	hydrochloric acid
H^+	hydrogen ion
H_2O_2	hydrogen peroxide
K_L (L/mg)	Langmuir model constant
q_m (mg/g)	maximum adsorption capacity
N	nitrogen
pzc	point of zero charge
K_i (mg/(g $min^{1/2}$))	rate constant for intra-particle diffusion model
K_1 (1/min)	rate constant for pseudo-first-order kinetic model
K_2 (g/(mg min))	rate constant for pseudo-second-order kinetic model
RB3R	reactive blue 3R
RB 49	reactive blue 49
RP4BN	red P4BN
SEM	scanning electron microscopy
NaCl	sodium chloride
NaOH	sodium hydroxide
Na^+	sodium ion
T	temperature
t (min)	time
UV-Vis	ultraviolet-visible
V (L)	volume
m (g)	weight
XRD	X-ray diffraction

Statement of Novelty

- It has been presented that more than one stable and possible composite can be prepared by testing different mass ratios of chitosan and hexagonal boron nitride.
- The characterization of the composites is presented comparatively depending on the changing mass composition.
- Removal behavior of the composites was examined and compared with each other.

References

[1] Vasiliev, V. V.; Morozov, E. V. Chapter 1 - Introduction. In *Advanced Mechanics of Composite Materials* (*Third Edition*); Eds. Vasiliev, V. V. Morozov, E. V.; (Elsevier, Amsterdam, Netherlands), 2013; pp. 1–27. DOI: 10.1016/B978-0-08-098231-1.00001-7.

[2] Carey, J. P. Introduction to Braided Composites. In *Handbook of Advances in Braided Composite Materials*; Carey, J. P., Ed.; (Elsevier, Amsterdam, Netherlands), 2017; pp. 1–21. DOI: 10.1016/B978-0-08-100369-5.00001-5.

[3] Knight, M.; Curliss, D. Composite Materials. In *Encyclopedia of Physical Science and Technology* (*Third Edition*); Ed. Meyers, R. A.; (Elsevier, Amsterdam, Netherlands), 2003; pp. 455–468. DOI: 10.1016/B0-12-227410-5/00128-9.

[4] Noor, A.; Khan, A.; Bhatti, H. N.; Zahid, M.; Aslam, F.; Naouar, A.; Al-Fawzan, F. F.; Alissa, S. A.; Iqbal, M. Polypyrrole and Rice Husk Composite Potential for the Adsorptive Removal of 2, 4, 6-Trichloro Phenol from Aqueous Medium. *Arab J. Chem.* 2022, *15*(12), 104352. DOI: 10.1016/j.arabjc.2022.104352.

[5] Han, M.; Zhang, C.; Ho, S. H. Immobilized Microalgal System: An Achievable Idea for Upgrading Current Microalgal Wastewater Treatment. *Environ. Sci. Ecotechnology*. 2023, *14*, 100227. DOI: 10.1016/j.ese.2022.100227.

[6] Rezai, B.; Allahkarami, E. Wastewater Treatment Processes—Techniques, Technologies, Challenges Faced, and Alternative Solutions. In *Soft Computing Techniques in Solid Waste and Wastewater Management*; Karri, R. R., Ravindran, G., and Dehghani, M. H., Eds.; (Elsevier, Amsterdam, Netherlands), 2021; pp. 35–53. DOI: 10.1016/B978-0-12-824463-0.00004-5.

[7] Karapanagioti, H. K. Water Management, Treatment and Environmental Impact. In *Encyclopedia of Food and Health*; Caballero, B., Finglas, P. M., and Toldrá, F., Eds.; (Elsevier, Amsterdam, Netherlands), 2016; pp. 453–457. DOI: 10.1016/B978-0-12-384947-2.00740-6.

[8] Moosavi, S.; Lai, C. W.; Gan, S.; Zamiri, G.; Akbarzadeh Pivehzhani, O.; Johan, M. R. Application of Efficient Magnetic Particles and Activated Carbon for Dye Removal from Wastewater. *ACS Omega*. 2020, *5*(33), 20684–20697. DOI: 10.1021/acsomega.0c01905.

[9] Singh, K.; Lataye, D. H.; Wasewar, K. L.; Yoo, C. K. Removal of Fluoride from Aqueous Solution: Status and Techniques. *Desalin. Water. Treat*. 2013, *51*(16–18), 3233–3247. DOI: 10.1080/19443994.2012.749036.

[10] Abd El-Ghany, N. A.; Elella, M. H. A.; Abdallah, H. M.; Mostafa, M. S.; Samy, M. Recent Advances in Various Starch Formulation for Wastewater Purification via Adsorption Technique: A Review. *J Polym. Environ*. 2023, 1–34. DOI: 10.1007/s10924-023-02798-x.

[11] Priyan, V. V.; Kumar, N.; Narayanasamy, S. Development of Fe3O4/CAC Nanocomposite for the Effective Removal of Contaminants of Emerging Concerns (Ce3+) from Water: An Ecotoxicological Assessment. *Environmental Pollution*. 2021, *285*, 285, 117326. DOI: 10.1016/j.envpol.2021.117326.

[12] Pourhakkak, P.; Taghizadeh, M.; Taghizadeh, A.; Ghaedi, M. A. *In Interface Science and Technology*; edited by, Hubbard, A. T.pp. 71–210. (Elsevier, Amsterdam, Netherlands), 2021. 10.1016/B978-0-12-818805-7.00009-6.

[13] Ali, I.; Alharbi, O. M.; ALOthman, Z. A.; Al-Mohaimeed, A. M.; Alwarthan, A. Modeling of Fenuron Pesticide Adsorption on CNTs for Mechanistic Insight and Removal in Water. *Environ. Res*. 2019, *170*, 389–397. DOI: 10.1016/j.envres.2018.12.066.

[14] Alqadami, A. A.; Wabaidur, S. M.; Jeon, B. H.; Khan, M. A. Co-Hydrothermal Valorization of Food Waste: Process Optimization, Characterization, and Water Decolorization Application. *Biomass Convers. Biorefin*. 2023, *2023*, 1–12. DOI: 10.1007/s13399-022-03711-7.

[15] Khan, M. A.; Otero, M.; Kazi, M.; Alqadami, A. A.; Wabaidur, S. M.; Siddiqui, M. R.; Alothman, Z. A.; Sumbul, S. Unary and Binary Adsorption Studies of Lead and Malachite Green Onto a Nanomagnetic Copper Ferrite/Drumstick Pod Biomass Composite. *J. Hazard. Mater*. 2019, *365*, 759–770. DOI: 10.1016/j.jhazmat.2018.11.072.

[16] Azam, M.; Wabaidur, S. M.; Khan, M. R.; Al-Resayes, S. I.; Islam, M. S. Heavy Metal Ions Removal from Aqueous Solutions by Treated Ajwa Date Pits: Kinetic, Isotherm, and Thermodynamic Approach. *Polymers*. 2022, *14*(5), 914. DOI: 10.3390/polym14050914.

[17] Nazari, M. T.; Schnorr, C.; Rigueto, C. V.; Alessandretti, I.; Melara, F.; da Silva, N. F.; Crestani, L.; Ferrari, V.; Vieillard, J.; Dotto, G. L., et al. A Review of the Main Methods for Composite Adsorbents Characterization. *Environ. Sci. Pollut. Res*. 2022, *29*(59), 1–19. DOI: 10.1007/s11356-022-23883-z.

[18] Rocky, K. A.; Pal, A.; Rupam, T. H.; Palash, M. L.; Saha, B. B. Recent Advances of Composite Adsorbents for Heat Transformation Applications. *Therm. Sci. Eng. Prog*. 2021, *23*, 100900. DOI: 10.1016/j.tsep.2021.100900.

[19] Ahmed, M. A.; Mohamed, A. A. The Use of Chitosan-Based Composites for Environmental Remediation: A Review. *Int J Biol Macromol*. 2023, 124787. DOI: 10.1016/j.ijbiomac.2023.124787.

[20] Sharma, V.; Shahnaz, T.; Subbiah, S.; Narayanasamy, S. New Insights into the Remediation of Water Pollutants Using Nanobentonite Incorporated Nanocellulose Chitosan Based Aerogel. *J Polym. Environ*. 2020, *28*(7), 2008–2019. DOI: 10.1007/s10924-020-01740-9.

[21] Bhimanapati, G. R.; Glavin, N. R.; Robinson, J. A. 2D Boron Nitride: Synthesis and Applications. In *Semiconductors and Semimetals*; Eds. Willardson, R. K. Beer, A. C.; (Elsevier, Amsterdam, Netherlands), 2016; pp. 101–147. DOI: 10.1016/bs.semsem.2016.04.004.

[22] Majety, S.; Cao, X. K.; Dahal, R.; Pantha, B. N.; Li, J.; Lin, J. Y.; Jiang, H. X. Semiconducting Hexagonal Boron Nitride for Deep Ultraviolet Photonics. In *Quantum Sensing and Nanophotonic Devices IX*; Razeghi, M., Tournie, E. Brown, G. J., (Eds.); SPIE Press: Washington USA, 2012; pp. 607–614. DOI: 10.1117/12.914084.

[23] Roy, S.; Zhang, X.; Puthirath, A. B.; Meiyazhagan, A.; Bhattacharyya, S.; Rahman, M. M.; Babu, G.; Susarla, S.; Saju, S. K.; Tran, M. K., et al. Properties and Applications of Two□Dimensional Hexagonal Boron Nitride. *Adv. Mater*. 2021, *33*(44), 2101589. DOI: 10.1002/adma.202101589.

[24] Dandil, S.; Düzgün, A. Effective Dye Adsorption with Cross-Linked Hexagonal Boron Nitride Spheres. *Bilgesci*. 2023, *7*(2), 95–104. DOI: 10.30516/bilgesci.1261182.

[25] Zafar, L.; Khan, A.; Kamran, U.; Park, S. J.; Bhatti, H. N. Eucalyptus (Camaldulensis) Bark-Based Composites for Efficient Basic Blue 41 Dye Biosorption from Aqueous Stream: Kinetics, Isothermal, and Thermodynamic Studies. *Surf. Interfaces*. 2022, *31*, 101897. DOI: 10.1016/j.surfin.2022.101897.

[26] Kamran, U.; Bhatti, H. N.; Noreen, S.; Tahir, M. A.; Park, S. J. Chemically Modified Sugarcane Bagasse-Based Biocomposites for Efficient Removal of Acid Red 1 Dye: Kinetics, Isotherms, Thermodynamics, and Desorption Studies. *Chemosphere*. 2022, *291*, 132796. DOI: 10.1016/j.chemosphere.2021.132796.

[27] c. https://dyeschemical.com/reactive-blue-49/, Accessed 05 06 2023

[28] Postai, D. L.; Demarchi, C. A.; Zanatta, F.; Melo, D. C. C.; Rodrigues, C. A. Adsorption of Rhodamine B and Methylene Blue Dyes Using Waste of Seeds of Aleurites Moluccana, a Low Cost Adsorbent. *Alex Eng J*. 2016, *55*(2), 1713–1723. DOI: 10.1016/j.aej.2016.03.017.

[29] Bakatula, E. N.; Richard, D.; Neculita, C. M.; Zagury, G. J. Determination of Point of Zero Charge of Natural

Organic Materials. *Environ. Sci. Pollut. Res.* 2018, *25*(8), 7823–7833. DOI: 10.1007/s11356-017-1115-7.

[30] Park, J. H.; Wang, J. J.; Xiao, R.; Wang, M.; Lee, Y. H.; Kang, S. W.; Seo, D. C. Characteristics of Adsorption Behavior of Potentially Toxic Metals by Biochar Derived from Fallen Leaves (Platanus) and Its Mechanism. *Sustain. Chem. Pharm.* 2022, *29*, 100776. DOI: 10.1016/j.scp.2022.100776.

[31] Aghdasinia, H.; Oskui, F. N.; Mirzaei, G.; Hosseini, S. S.; Sorkhabi, M. G. Nonlinear Kinetic Modeling of Malachite Green Adsorption Onto Green Waste Bio-Adsorbents Using CCF-RSM. *Chemom. Intell. Lab. Syst.* 2023, *240*, 104911. DOI: 10.1016/j.chemolab.2023.104911.

[32] Noor, S. N. M.; Hasnol, N. H.; Saufi, S. M. Isotherm and Kinetic of Adsorptive Purolite S108 Mixed Matrix Membrane for Boron Adsorption. *Mater. Today Proc.* 2023. DOI: 10.1016/j.matpr.2023.05.121.

[33] Değermenci, G. D.; Değermenci, N.; Ayvaoğlu, V.; Durmaz, E.; Çakır, D.; Akan, E. Adsorption of Reactive Dyes on Lignocellulosic Waste; Characterization, Equilibrium, Kinetic and Thermodynamic Studies. *J. Clean. Prod.* 2019, *225*, 1220–1229. DOI: 10.1016/j.jclepro.2019.03.260.

[34] Spoială, A.; Ilie, C. I.; Dolete, G.; Croitoru, A. M.; Surdu, V. A.; Truşcă, R. D.; Motelica, L.; Oprea, O. C.; Ficai, D.; Ficai, A., et al. Preparation and Characterization of Chitosan/TiO2 Composite Membranes as Adsorbent Materials for Water Purification. *Membranes.* 2022, *12* (8), 804. DOI: 10.3390/membranes12080804.

[35] Mosoarca, G.; Vancea, C.; Popa, S.; Gheju, M.; Boran, S. Syringa Vulgaris Leaves Powder a Novel Low-Cost Adsorbent for Methylene Blue Removal: Isotherms, Kinetics, Thermodynamic and Optimization by Taguchi Method. *Sci. Rep.* 2020, *10*(1), 17676. DOI: 10.1038/s41598-020-74819-x.

[36] Ighalo, J. O.; Adeniyi, A. G. A Mini-Review of the Morphological Properties of Biosorbents Derived from Plant Leaves. *Sn. Appl. Sci.* 2020, *2*(3), 509. DOI: 10.1007/s42452-020-2335-x.

[37] Bello, O. S. Adsorptive Removal of Malachite Green with Activated Carbon Prepared from Oil Palm Fruit Fibre by KOH Activation and CO_2 Gasification. *S. Afr. J. Chem. Eng.* 2013, *66*, 32–41. https://www.ajol.info/index.php/sajc/article/view/123094.

[38] Queiroz, M. F.; Teodosio Melo, K. R.; Sabry, D. A.; Sassaki, G. L.; Rocha, H. A. O. Does the Use of Chitosan Contribute to Oxalate Kidney Stone Formation? *Mar. Drugs.* 2014, *13*(1), 141–158. DOI: 10.3390/md13010141.

[39] Muinde, V.; Onyari, J. M.; Wamalwa, B. M.; Wabomba, J.; Nthumbi, R. M. Adsorption of Malachite Green from Aqueous Solutions Onto Rice Husks: Kinetic and Equilibrium Studies. *J. Environ. Prot.* 2017, *8*(3), 215–230. DOI: 10.4236/jep.2017.83017.

[40] Kenawy, E. R.; Ghfar, A. A.; Wabaidur, S. M.; Khan, M. A.; Siddiqui, M. R.; Alothman, Z. A.; Alqadami, A. A.; Hamid, M. Cetyltrimethylammonium Bromide Intercalated and Branched Polyhydroxystyrene Functionalized Montmorillonite Clay to Sequester Cationic Dyes. *J. Environ. Manage.* 2018, *219*, 285–293. DOI: 10.1016/j.jenvman.2018.04.121.

[41] Pylypchuk, I. V.; Kołodyńska, D.; Kozioł, M.; Gorbyk, P. P. Gd-DTPA Adsorption on Chitosan/Magnetite Nanocomposites. *Nanoscale Res. Lett.* 2016, *11*(1), 1–10. DOI: 10.1186/s11671-016-1363-3.

[42] Das, B.; Saikia, P.; Sharma, M.; Baruah, M. J.; Roy, S.; Bania, K. K. Direct Cyanidation of Silver Sulfide by Heterolytic C–CN Bond Cleavage of Acetonitrile. *R.S.C. Adv.* 2020, *10*(14), 8314–8318. DOI: 10.1039/D0RA00940G.

[43] Hadjiivanov, K. I.; Panayotov, D. A.; Mihaylov, M. Y.; Ivanova, E. Z.; Chakarova, K. K.; Andonova, S. M.; Drenchev, N. L. Power of Infrared and Raman Spectroscopies to Characterize Metal-Organic Frameworks and Investigate Their Interaction with Guest Molecules. *Chem. Rev.* 2020, *121*(3), 1286–1424. DOI: 10.1021/acs.chemrev.0c00487.

[44] Dara, P. K.; Mahadevan, R.; Digita, P. A.; Visnuvinayagam, S.; Kumar, L. R.; Mathew, S.; Ravishankar, C. N.; Anandan, R. J. S. A. S. Synthesis and Biochemical Characterization of Silver Nanoparticles Grafted Chitosan (Chi-Ag-NPs): In vitro Studies on Antioxidant and Antibacterial Applications. *Sn. Appl. Sci.* 2020, *2*(4), 1–12. DOI: 10.1007/s42452-020-2261-y.

[45] Budnyak, T. M.; Pylypchuk, I. V.; Tertykh, V. A.; Yanovska, E. S.; Kolodynska, D. Synthesis and Adsorption Properties of Chitosan-Silica Nanocomposite Prepared by Sol-Gel Method. *Nanoscale Res. Lett.* 2015, *10*(1), 1–10. DOI: 10.1186/s11671-014-0722-1.

[46] Ramesh, J.; Salman, A.; Hammody, Z.; Cohen, B.; Gopas, J.; Grossman, N.; Mordechai, S. FTIR Microscopic Studies on Normal and H-Ras Oncogene Transfected Cultured Mouse Fibroblasts. *Eur. Biophys. J.* 2001, *30*(4), 250–255. DOI: 10.1007/s002490100137.

[47] Sudeep, P. M.; Vinod, S.; Ozden, S.; Sruthi, R.; Kukovecz, A.; Konya, Z.; Vajtai, R.; Anantharaman, M. R.; Ajayan, P. M.; Narayanan, T. N. Functionalized Boron Nitride Porous Solids. *R.S.C. Adv.* 2015, *5*(114), 93964–93968. DOI: 10.1039/C5RA19091F.

[48] Litefti, K.; Freire, M. S.; Stitou, M.; González-Álvarez, J. Adsorption of an Anionic Dye (Congo Red) from Aqueous Solutions by Pine Bark. *Sci. Rep.* 2019, *9*(1), 16530. DOI: 10.1038/s41598-019-53046-z.

[49] Yin, Y.; Yin, H.; Wu, Z.; Qi, C.; Tian, H.; Zhang, W.; Hu, Z.; Feng, L. Characterization of Coals and Coal Ashes with High Si Content Using Combined Second-Derivative Infrared Spectroscopy and Raman Spectroscopy. *Crystals.* 2019, *9*(10), 513. DOI: 10.3390/cryst9100513.

[50] Stagner, W. C.; Gaddam, S.; Parmar, R.; Ghanta, A. K. Chapter Five - Sucrose octaacetate. In *Profiles of Drug Substances, Excipients and Related Methodology*; Brittain, H. G., Ed.; (Elsevier, Amsterdam, Netherlands), 2019; pp. 267–291. DOI: 10.1016/bs.podrm.2019.02.002.

[51] Jin, Z.; Cui, W.; Zhang, F.; Wang, F.; Cheng, S.; Fu, Y.; Huang, A. Rapid Identification for the Pterocarpus Bracelet by Three-Step Infrared Spectrum Method. *Molecules.* 2022, *27*(15), 4793. DOI: 10.3390/molecules27154793.

[52] Fatoni, A.; Hariani, P. L.; Hermansyah, H.; Lesbani, A. Synthesis and Characterization of Chitosan Linked by Methylene Bridge and Schiff Base of 4, 4-Diaminodiphenyl Ether-Vanillin. *Indones. J. Chem.* 2018, *18*(1), 92–101. DOI: 10.22146/ijc.25866.

[53] Jozanikohan, G.; Abarghooei, M. N. The Fourier Transform Infrared Spectroscopy (FTIR) Analysis for the Clay Mineralogy Studies in a Clastic Reservoir. *J. Pet. Explor. Prod. Technol.* 2022, *12*(8), 1–14. DOI: 10.1007/s13202-021-01449-y.

[54] Ali, M. E. A.; Aboelfadl, M. M. S.; Selim, A. M.; Khalil, H. F.; Elkady, G. M. Chitosan Nanoparticles Extracted from Shrimp Shells, Application for Removal of Fe (II) and Mn (II) from Aqueous Phases. *Sep. Sci. Technol.* 2018, *53*(18), 2870–2881. DOI: 10.1080/01496395.2018.1489845.

[55] Huang, C.; Chen, C.; Ye, X.; Ye, W.; Hu, J.; Xu, C.; Qiu, X. Stable Colloidal Boron Nitride Nanosheet Dispersion and Its Potential Application in Catalysis. *J. Mater. Chem. A.* 2013, *1*(39), 12192–12197. DOI: 10.1039/C3TA12231J.

[56] Rey, C.; Combes, C.; Drouet, C.; Grossin, D. Bioactive Ceramics: Physical Chemistry. In *Comprehensive Biomaterials*; Ed. Ducheyne, P.; (Elsevier, Amsterdam, Netherlands), 2011; pp. 187–221. DOI: 10.1016/B978-0-08-055294-1.00178-1.

[57] Arab, C.; El Kurdi, R.; Patra, D. Effect of pH on the Removal of Anionic and Cationic Dyes Using Zinc Curcumin Oxide Nanoparticles as Adsorbent. *Mater. Chem. Phys.* 2022, 277, 125504. DOI: 10.1016/j.matchemphys.2021.125504.

[58] El Haddad, M.; Mamouni, R.; Saffaj, N.; Lazar, S. Removal of a Cationic Dye–Basic Red 12–From Aqueous Solution by Adsorption Onto Animal Bone Meal. *J. Assoc. Arab Univ. Basic Appl. Sci.* 2012, *12*(1), 48–54. DOI: 10.1016/j.jaubas.2012.04.003.

[59] Katenta, J.; Nakiguli, C.; Mukasa, P.; Ntambi, E. Removal of Chromium (VI) from Tannery Effluent Using Bio-Char of Phoenix Reclinata Seeds. *Green Sustain. Chem.* 2020, *10*(3), 91. DOI: 10.4236/gsc.2020.103007.

[60] Akin Sahbaz, D.; Dandil, S.; Acikgoz, C. Adsorption of Reactive Blue 49 Onto Cross-Linked Chitosan-Based Composites Containing Waste Mussel Shell and Waste Active Sludge Char. *Water Sci. Technol.* 2021, *83*(3), 715–726. DOI: 10.2166/wst.2021.008.

[61] Akın Şahbaz, D.; Dandıl, S.; Açıkgöz, Ç. Kinetic Studies on the Removal of Reactive Blue 49 Dye from Aqueous Solution Onto Chitosan-Activated Sludge Composite Particles. *Bio. Chem. Res.* 2018, *6*, 19–29.

[62] Bouhadjra, K.; Barras, A.; Lemlikchi, W.; Addad, A.; Das, M. R.; Amin, M. A.; Szunerits, S.; Boukherroub, R. Phytic Acid-Doped Poly-N-Phenylglycine Potato Peels for Removal of Anionic Dyes: Investigation of Adsorption Parameters. *New. J. Chem.* 2022, *46*(11), 5111–5120. DOI: 10.1039/D1NJ04713B.

[63] Akar, S. T.; Gorgulu, A.; Kaynak, Z.; Anilan, B.; Akar, T. Biosorption of Reactive Blue 49 Dye Under Batch and Continuous Mode Using a Mixed Biosorbent of Macro-Fungus Agaricus Bisporus and Thuja orientalis Cones. *Chem. Eng. J.* 2009, *148*(1), 26–34. DOI: 10.1016/j.cej.2008.07.027.

[64] Tosun Satır, I.; Sayin, F.; Gedikbey, T.; Tunali Akar, S. A Novel Sorbent for Removal of Reactive Textile Dye: TDPA-KCl. *Environ. Sci. Pollut. Res.* 2019, *26*(23), 23279–23291. DOI: 10.1007/s11356-019-05466-7.

[65] Asgher, M.; Bhatti, H. N. Removal of Reactive Blue 19 and Reactive Blue 49 Textile Dyes by Citrus Waste Biomass from Aqueous Solution: Equilibrium and Kinetic Study. *Can. J. Chem. Eng.* 2012, *90*(2), 412–419. DOI: 10.1002/cjce.20531.

[66] Akar, S. T.; Gorgulu, A.; Akar, T.; Celik, S. Decolorization of Reactive Blue 49 Contaminated Solutions by Capsicum Annuum Seeds: Batch and Continuous Mode Biosorption Applications. *Chem. Eng. J.* 2011, *168*(1), 125–133. DOI: 10.1016/j.cej.2010.12.049.

[67] Badawi, A. K.; Abd Elkodous, M.; Ali, G. A. Recent Advances in Dye and Metal Ion Removal Using Efficient Adsorbents and Novel Nano-Based Materials: An Overview. *R.S.C. Adv.* 2021, *11*(58), 36528–36553. DOI: 10.1039/D1RA06892J.

[68] Saha, D.; Grappe, H. A. Adsorption Properties of Activated Carbon Fibers. In *Activated Carbon Fiber and Textiles*; Ed. Chen, J. Y.; (Woodhead Publishing, Cambridge, England), 2017; pp. 143–165. DOI: 10.1016/B978-0-08-100660-3.00005-5.

[69] Shah, G.; Sahota, S.; Vijay, V. K.; Pant, K. K.; Ghosh, P. Recent Developments in Pressure Swing Adsorption for Biomethane Production. In *Emerging Technologies and Biological Systems for Biogas Upgrading*, Eds. Aryal, N., Ottosen, L. D. M.; Kofoed, M. V. W., and Pant, P. (Elsevier, Amsterdam, Netherlands), 2021; pp. 93–116. DOI: 10.1016/B978-0-12-822808-1.00005-2.

[70] Wu, F. C.; Tseng, R. L.; Juang, R. S. Initial Behavior of Intraparticle Diffusion Model Used in the Description of Adsorption Kinetics. *Chem. Eng. J.* 2009, *153*(1–3), 1–8. DOI: 10.1016/j.cej.2009.04.042.

[71] Nakama, Y. S.; *In Cosmetic Science and Technology*; (Elsevier, Amsterdam, Netherlands): 2017pp. 231–244. DOI:10.1016/B978-0-12-802005-0.00015-X.

[72] Dawodu, F. A.; Akpomie, G. K.; Abuh, M. A. Equilibrium Isotherm Studies on the Batch Sorption of Copper (II) Ions from Aqueous Solution Unto Nsu Clay. *Int. J. Sci. Eng. Res.* 2012, *3*(12), 1–7.

[73] Baldez, E. E.; Robaina, N. F.; Cassella, R. J. Study of Rhodamine B Retention by Polyurethane Foam from Aqueous Medium in Presence of Sodium Dodecylsulfate. *Sep. Sci. Technol.* 2009, *44*(13), 3128–3149. DOI: 10.1080/01496390903182396.

[74] Ebelegi, A. N.; Ayawei, N.; Wankasi, D. Interpretation of Adsorption Thermodynamics and Kinetics. *Open J. Phys. Chem.* 2020, *10*(3), 166. DOI: 10.4236/ojpc.2020.103010.

[75] Junior, R. A. F.; Frescura, L. M.; de Menezes, B. B.; de Moraes Bastos, A. F.; da Rosa, M. B. Adsorption of Naphthalene and Its Derivatives Onto High-Density Polyethylene Microplastic: Computational, Isotherm, Thermodynamic, and Kinetic Study. *Environ. Pollut.* 2023, *318*, 120919. DOI: 10.1016/j.envpol.2022.120919.

[76] de Oliveira, T. F.; de Souza, C. P.; Lopes-Moriyama, A. L.; da Silva, M. L. P. In situ Modification of MCM-41 Using Niobium and Tantalum Mixed Oxide from Columbite Processing for Methylene Blue Adsorption: Characterization, Kinetic, Isotherm, Thermodynamic

and Mechanism Study. *Mater. Chem. Phys.* 2023, *294*, 127011. DOI: 10.1016/j.matchemphys.2022.127011.

[77] Raghav, S.; Kumar, D. Adsorption Equilibrium, Kinetics, and Thermodynamic Studies of Fluoride Adsorbed by Tetrametallic Oxide Adsorbent. *J. Chem. Eng, Data*. 2018, *63*(5), 1682–1697. DOI: 10.1021/acs.jced.8b00024.

[78] Tu, Y. J.; You, C. F.; Zhang, Z.; Duan, Y.; Fu, J.; Xu, D. Strontium Removal in Seawater by Means of Composite Magnetic Nanoparticles Derived from Industrial Sludge. *Water*. 2016, *8*(8), 357. DOI: 10.3390/w8080357.

[79] Di, J.; Ruan, Z.; Zhang, S.; Dong, Y.; Fu, S.; Li, H.; Jiang, G. Adsorption Behaviors and Mechanisms of Cu^{2+}, Zn^{2+} and Pb^{2+} by Magnetically Modified Lignite. *Sci. Rep*. 2022, *12*(1), 1394. DOI: 10.1038/s41598-022-05453-y.